Journal of Magnetism and Magnetic Materials 393 (2015) 226–232

Contents lists available at ScienceDirect

Journal of Magnetism and Magnetic Materials

journal homepage: www.elsevier.com/locate/jmmm

Surface states of FeF_2 (110) and its uncompensated magnetization

F. Munoz [a,b], A.H. Romero [c], J. Mejía-López [d,b], Igor V. Roshchin [e,f], R.I. González [a,b], M. Kiwi [a,b,*]

[a] Departamento de Física, Facultad de Ciencias, Universidad de Chile, Casilla 653, Santiago 7800024, Chile
[b] Centro para el Desarrollo de la Nanociencia y la Nanotecnología, CEDENNA, Avda. Ecuador 3493, Santiago 9170124, Chile
[c] Physics Department, West Virginia University, Morgantown, WV 26506-6315, USA
[d] Facultad de Física, Universidad Católica de Chile, Casilla 306, Santiago 7820436, Chile
[e] Department of Physics and Astronomy, Texas A&M University – College Station, TX 77843-4242, USA
[f] Department of Materials Science and Engineering, Texas A&M University – College Station, TX 77843-3003, USA

ARTICLE INFO

Article history:
Received 14 October 2014
Received in revised form
13 May 2015
Accepted 24 May 2015
Available online 5 June 2015

ABSTRACT

The (110) surface of iron fluoride (FeF_2) is especially relevant to the understanding of the exchange bias phenomenon, which has important applications in the sensor industry, and has been extensively explored, both theoretically and experimentally. Here we investigate this FeF_2 surface by means of *ab initio* techniques. We compute the (110) surface reconstruction, energetics, magnetic moments, band structure, charge density and electron localization function, for the two possible terminations (Fe and F). The surface reconstruction modifies the atomic and electronic structure of the free surface, yielding magnetism of a magnitude of $0.1\mu_B$ per surface unit cell. Moreover, the charge density also changes, which alters the bonding in the vicinity of the surface. All these changes are expected to be relevant for exchange bias, that is once a ferromagnetic layer is deposited on the FeF_2 surface.

1. Introduction

For almost 60 years, exchange bias (EB) has attracted the attention of theorists, experimentalists and engineers. Besides its fundamental interest, understanding the EB mechanism is relevant for such applications as magnetic sensors and magnetic memories [1–3], and has been a long standing challenge for theorists and experimentalists, since Meiklejohn and Bean [4,5] discovered EB in 1956. This phenomenon manifests itself as a shift of the center of the magnetization loop, M vs. H, away from the origin. Iron fluoride (FeF_2) and especially its (110) surface have been extensively investigated experimentally [3]. Also, it has been instrumental to develop theoretical models [6], which mostly rely on the presence of an uncompensated magnetization at or near the surface. Actually, several experimental studies have demonstrated the presence of this magnetization in the vicinity of the FeF_2 surface [7–16].

To understand the origin of this uncompensated magnetization, careful theoretical modeling of the surface is needed. To the best of our knowledge not much is known about the details of the surface electronic and magnetic structure, and how it differs from the bulk. Our goal is to understand the surface states (SS) and their characteristics, primarily their electronic and magnetic properties, and to see how this can lead to the generation of uncompensated magnetization near the surface [17,18].

This paper is organized as follows: After this Introduction, in Section 2, we discuss our physical model and the way to treat it. In Section 3 the results of our calculations are presented: energies and magnetic moments, band structure, charge density and electron localization function. Finally, in Section 4 we summarize and draw conclusions.

2. Model and calculation method

2.1. Surface model

Bulk iron fluoride (FeF_2) has a body centered tetragonal (rutile) structure, with the space group $P4/mnm$ as illustrated in Fig. 1(a). Its lattice parameters are $a=4.70$ Å and $c=3.31$ Å. The iron atoms are octahedrally coordinated, but they form a distorted octahedron, with two F atoms ≈ 2.03 Å apart from their first neighbor Fe atoms, while the remaining F atoms are at a distance of ≈ 2.15 Å from the Fe atoms. This Jahn–Teller distortion is correlated to changes in the spin polarization along the Fe–F bond [19].

As the focus of our interest we have chosen the (110) surface (illustrated in Fig. 1(b)), since experimentally it is the most intensively studied one [3,6,20–25]. Despite being a magnetically

* Corresponding author at: Departamento de Física, Facultad de Ciencias, Universidad de Chile, Casilla 653, Santiago 7800024, Chile. Fax: +562 2271 2973.

http://dx.doi.org/10.1016/j.jmmm.2015.05.064
0304-8853/

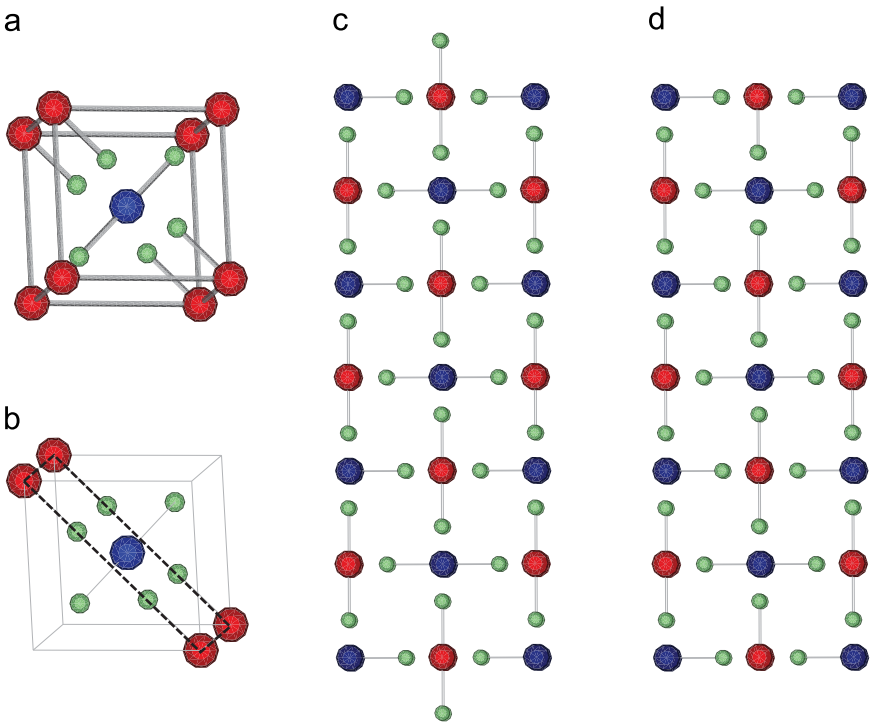

Fig. 1. (a) Conventional FeF_2 unit cell. Blue and red denote iron atoms of opposite magnetic moment orientations. The F atoms are shown in green. (b) Illustration of the (110) layer. The (110) surface terminations we investigated are: (c) F terminated and (d) Fe terminated. (For interpretation of the references to color in this figure caption, the reader is referred to the web version of this paper.)

compensated surface (*i.e.*, one up and one down spin per surface layer unit cell), this orientation exhibits a remarkably large EB field [6,3,25]. Here we have limited our attention to two possible surface terminations: fluorine (Fig. 1(c)) and iron terminated (Fig. 1 (d)). While for the former the Fe surface ions keep all their nearest neighbors, for the latter the topmost F atoms are absent (non-stoichiometric surface). Actually, these topmost F atom dangling bonds are saturated by fluorine, which form F_2 dimers.

In order not to make the computational labor too extensive we modeled the system by means of a slab geometry. Strictly speaking, to obtain a surface state (SS) semi-infinite boundary conditions are required along the surface plane. However, a slab that is sufficiently thick can be used to properly model the bulk. For metallic systems the electronic states have a large penetration depth and can even tunnel from one side of the slab to the other. However, the insulator FeF_2 states are well localized, and therefore the thickness of the slab is not an issue. To check whether the surface and bulk-like states are accurately obtained we varied the slab thickness from ≈ 7.5 Å (2 layers) to ≈ 24.4 Å (7 layers), using a one-layer increment. The whole slab was relaxed until all the atomic forces were less than 0.02 eV/Å. For four layer slabs or thicker we found both bulk and SS-like states.

2.2. Computational details

The calculations were performed *ab initio* using the density functional theory (DFT) as implemented in the VASP Package [26,27]. The energy cutoff of the plane waves was set to the rather large value of 500 eV to achieve reasonable completeness of the basis set. We used the Perdew–Burke–Ernzerhof (PBE) exchange-correlation parametrization [28]. Projector augmented wave (PAW) pseudopotentials were employed [29,30]. However, because of the significant electronic correlation, both the local density approximation (LDA) and the generalized gradient approximation (GGA) fail to yield a realistic description [31]. There are several reasons for this failure: (i) LDA and GGA functionals tend to over-delocalize electrons, (ii) the on-site Coulomb repulsion U is ignored, and (iii) the electrons see their own self-interaction potential.

To partially overcome these shortcomings the GGA+U method (Dudarev's approach [32]) is used to treat these highly correlated Fe d-orbitals. The parameters are taken from the work by López-Moreno et al. [19], and the results that are obtained compare favorably both with other theoretical methods [33], and with some of the available experimental data [34].

To be on the safe side, we performed a careful calculation of the bulk energy bands, which yields agreement with the results reported previously [19], and also with experimental data [35]. For the bulk a $20 \times 20 \times 29$ k-point mesh was used, while for the (110) orientation a $14 \times 29 \times 14$ mesh was implemented, in combination with the tetrahedron method, and Blöchl corrections [36]. For the length of the lattice parameters we obtain $a=4.80$ Å and $c=3.32$ Å, which compare well with $a=4.70$ Å and $c=30.31$ Å, the values obtained experimentally by Strempfer et al. [37]

The k-point mesh used for the slab calculations is $14 \times 29 \times 1$. But, since the SS can be metallic, the electronic occupancy was calculated incorporating a Gaussian smearing (of width 0.01 eV). Magnetic moments were calculated by integrating the magnetization density inside a Wigner–Seitz sphere of radius 1.3 Å, centered around every Fe atom.

The layer-resolved band structure calculations are made projecting the wavefunction onto spherical harmonics centered on each atom (Wigner–Seitz sphere). To simplify the discussion of the different spin orientations, and to make them directly accessible from the figures, in what follows the spin component will be labeled as 'red' and 'blue', instead of the conventional 'up' and 'down'.

3. Results and discussion

Surface relaxation plays a significant role here. However, its effect is different for the two surface terminations discussed

above. The atomic configurations resulting from the surface relaxation are presented for both terminations in Fig 2. The largest displacements occur for the stoichiometric F-terminated surface, since there is a noticeable change in the position of the Fe atoms in the first and the second layer (we will denominate the latter as subsurface layer). In fact, there is a zig-zag reconstruction, with half of the Fe atoms displaced 0.2 Å above their nominal bulk position, and the other half displaced about the same amount below that reference position. The Fe-terminated surface shows a similar, but much smaller reconstruction. However, in both cases the F–Fe bond length remains close to its bulk value (2.04 Å).

It is noteworthy that these results are for the calculations that assume an atomically smooth surface. When this is not the case, which often happens in experimental systems, these irregularities can spread over a larger thickness due to the surface roughness. Moreover, it is possible that it would be amplified due to the additional missing bonds of some of the Fe atoms. While modeling this effect would be very interesting for the description of the experimental systems, which is beyond the scope of this work.

3.1. Energy calculations

The surface energy per area unit, E_S^F and E_S^{Fe}, for F and Fe terminations are displayed in Fig. 3(a), and were calculated as

$$E_S^F = \frac{E_{\text{slab}} - N\,E_{\text{bulk}}}{2A}, \tag{1}$$

$$E_S^{Fe} = \frac{E_{\text{slab}} + E_{F_2} - N\,E_{\text{bulk}}}{2A}, \tag{2}$$

where N is the number of layers in the slab, A is the lateral unit cell area, the factor of two is due to the fact that the slab has two free surfaces, and the extra term in Eq. (2) is the energy of a F dimer. The usual expression for surface energy has to be used for the F-terminated surface (Eq. (1)). However, since the Fe-terminated surface is non-stoichiometric the missing F atoms form a free-standing dimer, and have to be included in the energy balance (Eq. (2)). Both surface terminations show almost no dependence of the surface energy as a function of slab thickness, and the value of E_S approaches E_S=0.09 eV for the F-terminated surface, and E_S=0.27 eV for the Fe-termination. Such a large value of E_S for the non-stoichiometric surface is due to the strong F–Fe bonding. Despite its large E_S energy it may be found in Fe deposition experiments, in sub-monolayer form.

3.2. Band structure and magnetic moment

For the band structure analysis, it is convenient to start by looking at the bulk (110) band structure, displayed in Fig. 4(a). We note that FeF_2 shows a large band gap, of about 4 eV. At the Γ point, the bottom of the conduction band has two spin-degenerate s-like states. As this band approaches the Brillouin zone X point, and also over all of the Brillouin zone boundary, both states are spin-split, and they adopt $d_{x^2+y^2}$ and d_{z^2} orbital character for the blue and red spin components, respectively. The top of the valence band has two almost spin-degenerate flat d-bands, and they correspond to a d_{z^2} and $d_{x^2+y^2}$ orbital decomposition for blue and red spin orientations, respectively. These orientations are opposite to the conduction bands spin orientations mentioned above. The states discussed so far are strongly projected on Fe atoms. The

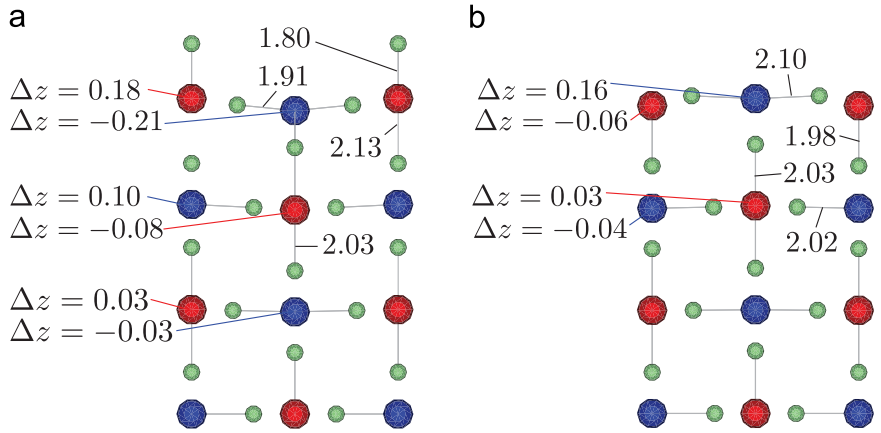

Fig. 2. (a) F-terminated and (b) Fe-terminated surfaces after atomic relaxation. Δz is the displacement of Fe atoms relative to the bulk equilibrium geometry, and the nearest F–Fe distances are also provided. When $\Delta z = 0$ or when the F–Fe bonds have the equilibrium distance (2.04 Å) these quantities are omitted. The upper layer is the surface.

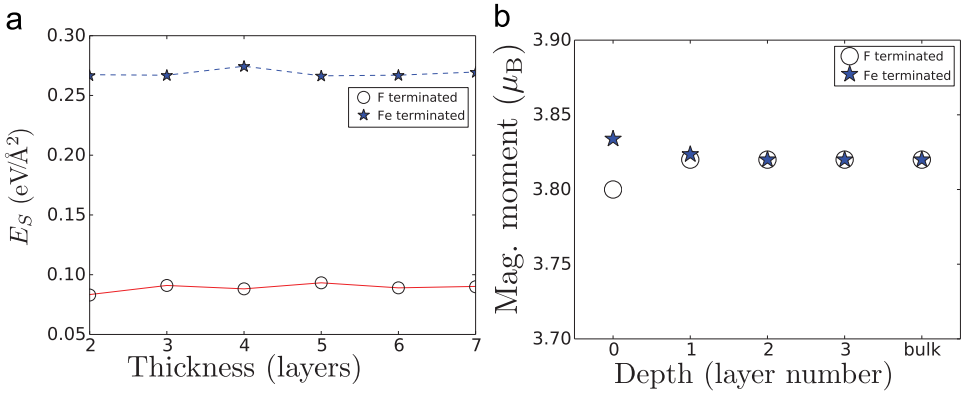

Fig. 3. (a) Surface energy (E_s) vs. slab thickness. (b) Magnetic moment vs. depth (the surface layer corresponds to the depth equal to 0).

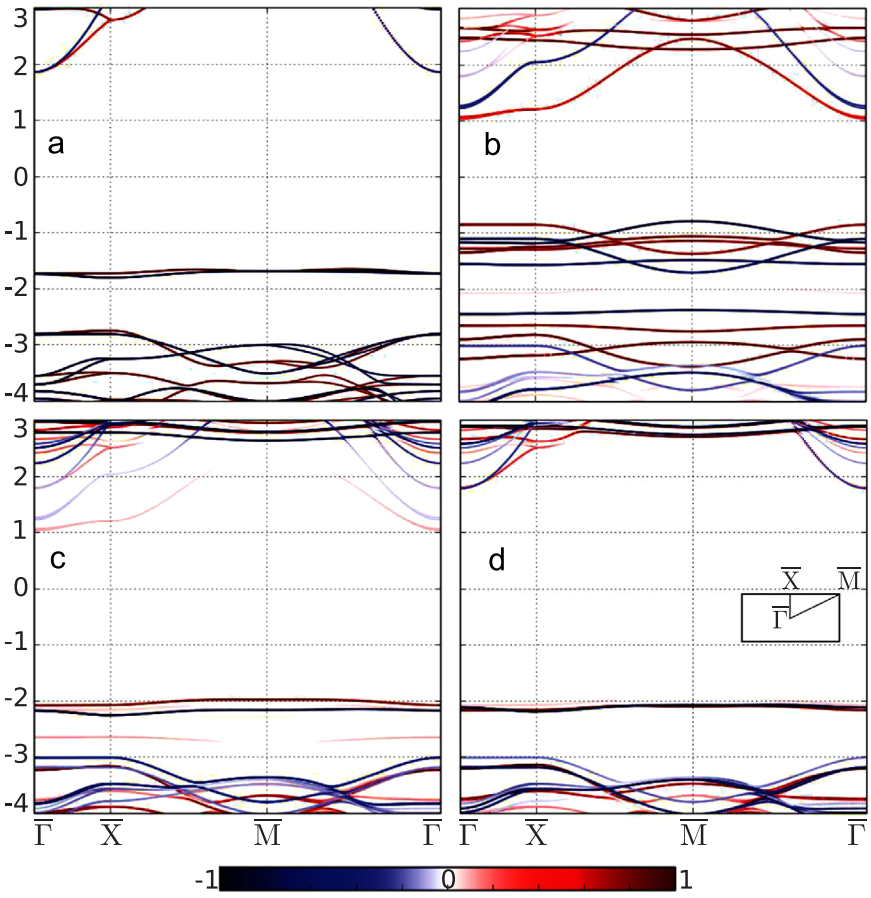

Fig. 4. Layer-resolved band structure for (a) the bulk along the (110) direction, (b)–(d) the F-terminated surface, sub-surface (second layer), and third sub-surface layer, respectively. The color intensity scale indicates the magnitude of the projection of each state on the respective layer. The colors (red and blue) distinguish the two spin projections. The inset in (d) indicates the relevant points of the 2D Brillouin zone. (For interpretation of the references to color in this figure caption, the reader is referred to the web version of this paper.)

other states shown, for lower energies, belong to mixed Fe-d and F-p states.

From the bulk band structure it is apparent that a (110) surface (with z pointing out-of-plane, along [110]) will induce an energy gap between the $d_{x^2+y^2}$ and d_{z^2} bands. This, in turn, will spin-split both the valence and conduction bands. Indeed, such spin-splitting happens for both surface terminations. This could be relevant for the occurrence of exchange bias, when a ferromagnet such as Fe, Ni, or Co is deposited on FeF_2 surface. However, it is convenient to look first at what happens to the inner layers (similar to the bulk). Here we limit our attention to the FeF_2 surface, and the case of a ferromagnet/FeF_2 system will be the subject matter of forthcoming publication.

Let us start with the band structure of the F-terminated surface. The third layer from the surface, Fig. 4(d), has a band structure that looks very similar to the bulk, but with lower energies (since E_F increases due the SS). Neither the valence nor the conduction bands exhibit the aforementioned spin-splitting, and also no SS can be observed. The subsurface band structure (layer adjacent to the surface layer, Fig. 4(c)) also resembles the bulk states, but the valence d-bands (at ~ -2 eV) have a small spin-splitting of ~0.1 eV. In this layer, some of the conduction band SS also penetrate weakly (soft colors in the gap). Finally, the surface layer, Fig. 4 (b), has several SS: six states (between -1 and -3 eV) are F atom states of p-character (at the top), two states are the Fe $d_{x^2+y^2}$ and d_{z^2} bands, and the gap between them is about 1.5 eV. Consequently, a large splitting between both spin components does emerge. The conduction s–d band is lower in energy than its bulk counterpart, and it presents a remarkable difference between both spin components. It is noteworthy that the strong localization of the SS does validate the slab model used in our calculations.

The band structure of the Fe-terminated surface and subsurface layers are shown in Fig. 5. The subsurface layer band structure are quite similar to the true bulk, however the valence bands display a small spin-splitting (~0.1 eV at $\bar{\Gamma}$), and in the conduction region bulk- and SS-like states coexist, albeit both with small intensity. The surface layer shows a major difference relative to the F-terminated surface: the s–d SS are metallic. Besides the fact that the electronic transport resides on the surface, it also implies that the spin occupations no longer need to be integers (Fermi surface), and therefore there is no obstacle for them to develop a net magnetic moment, as shown in Fig. 5(a), where the red (blue) spin component corresponds to the majority (minority). For this termination the difference in the occupations implies a net magnetization of $\sim 0.1\mu_B$ per lateral unit cell.

The magnetic moment (Fig. 3(b)) adopts a value that is quite close to the bulk, even for the surface layer. Beyond the sub-surface layer, its magnitude remains almost constant. There is no net magnetization on the F-terminated surface, however the Fe-terminated surface has a net magnetic moment of $0.1\mu_B$ per lateral unit cell. The latter magnetic moment is itinerant on the surface layer, and decays exponentially away from the surface.

3.3. Piezomagnetic response

Several previous publications have proposed [38–40] that an external strain applied to FeF_2 can change its magnetic properties

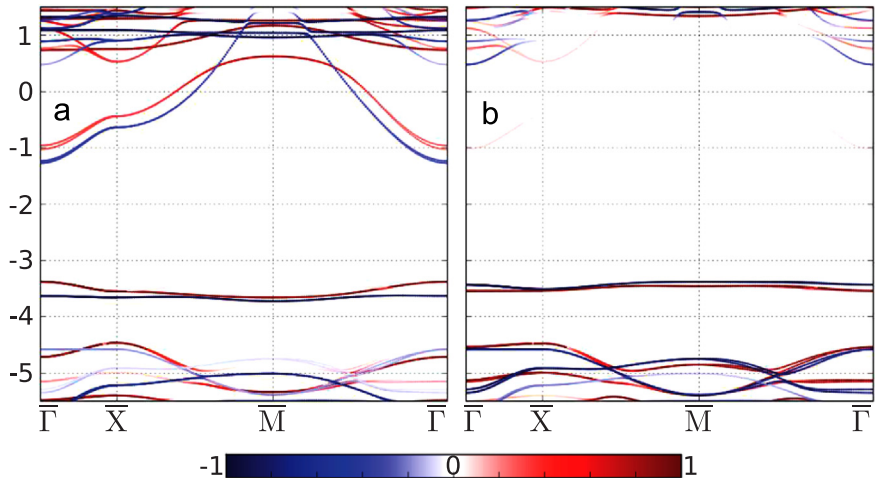

Fig. 5. Layer-resolved band structure of the Fe-terminated (a) surface and (b) sub-surface layers. For the meaning of the labels see the caption of Fig. 4. (For interpretation of the references to color in this figure caption, the reader is referred to the web version of this paper.)

due to piezomagnetic coupling. However, we are not aware of any systematic studies, experimental or theoretical, that clearly demonstrates this effect. For CoF_2 and MnF_2, the piezomagnetic effect was measured experimentally [41]. A very recent attempt has been made to perform calculations for the piezomagnetic effect [42] in CoF_2. With our slab geometry we have mimicked this effect by scaling the lateral lattice parameters, while keeping the vector normal to the (110) surface constant, and relaxing the forces and atomic positions.

The net magnetic moment (due to the SS) of an Fe-terminated surface (Fig. 6(a)) quickly decreases when the compression reaches 2%, and there is no net magnetization for a compression larger than 4%. When the system is stretched there is a significant initial magnetization increase in the Fe terminated surface layers, which changes slope beyond a 1% expansion. All in all, the system increases (reduces) its magnetic moment per lateral unit cell by $0.1\mu_B$ when the stretching (compression) reaches 4%. These magnetization variations could become important for a bilayer system with lattice mismatch, like FeF_2/TM, where TM=Fe, Ni or Co, for example. The F-terminated surface has no net magnetization within the strain range studied. The magnetic moment per iron atom is shown in Fig. 6(b). Regardless of the surface termination, the strain slightly changes the magnetic moment of the Fe atoms in the subsurface layer. Such a behavior is expected since both terminations have a similar electronic structure (which also is close to the bulk one). The surface layer of the F-terminated surface has a lower atomic magnetic moment, but it follows the same trend as the atoms lying further away from the surface. On the Fe-terminated surface, Fe atoms have a magnetic moment that is larger than the bulk one, when no external strain is applied. This is due to the fact that they have a reduced coordination number.

3.4. Charge density and electron localization function

The charge density of Fig. 7 shows that the basic 'building block' of FeF_2 are the F–Fe–F trimers. The symmetry breaking induced by the surface creates a large electron localization for the Fe terminated surface. Interestingly enough, there is a formation of tubular basins (nanowire-like) running along the [010] direction, which is saturated by the F–Fe bonds for the Fe-terminated surface. This indicates that for the Fe surface there is a large surface reactivity, in the direction right in the middle of the Fe–Fe bond, along the [010] direction. This happens to be at 1.6 Å from the atom closest to the surface Fe atom. Therefore, a delocalized electronic state extend along this direction, which comes from

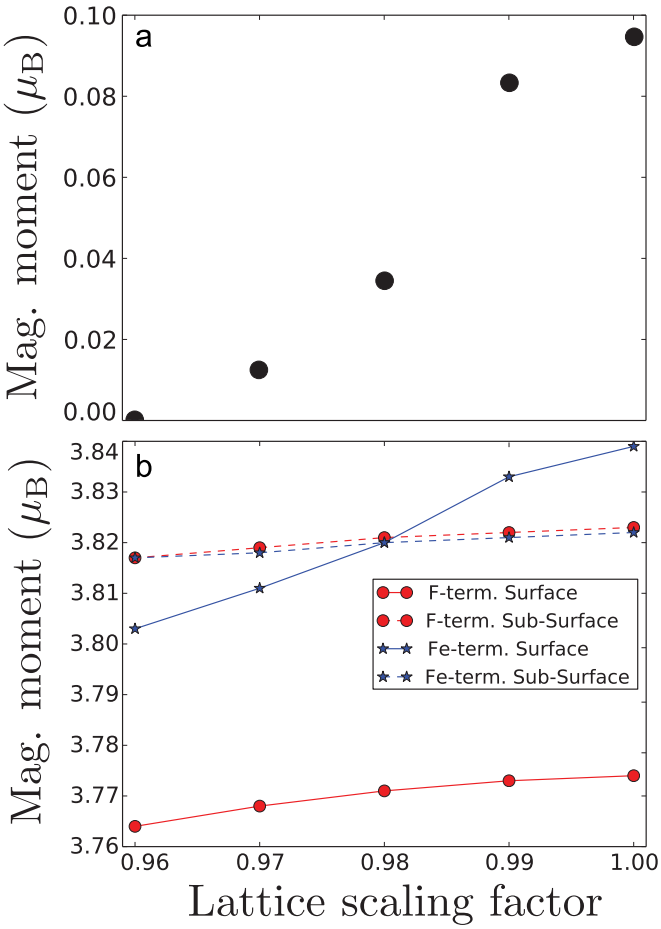

Fig. 6. (a) Net magnetization per lateral unit cell of an Fe-terminated surface as a function of the lateral compression. (b) Surface and subsurface magnetic moment of the Fe atoms as a function of compression, for both surface terminations.

quasi-free electrons from the unsaturated Fe as it is clearly seen in Fig. 7(d). This peculiar basin lies above the Fe atom that has its two first neighbors forming a trimer. There are no observable changes below the surface layer. For the F-terminated case there is a strong bonding between the topmost F and it closest Fe atom, but at the expense of a weaker bond of this Fe with the rest of the F atoms. The Fe-terminated surface presents a more complicated scenario,

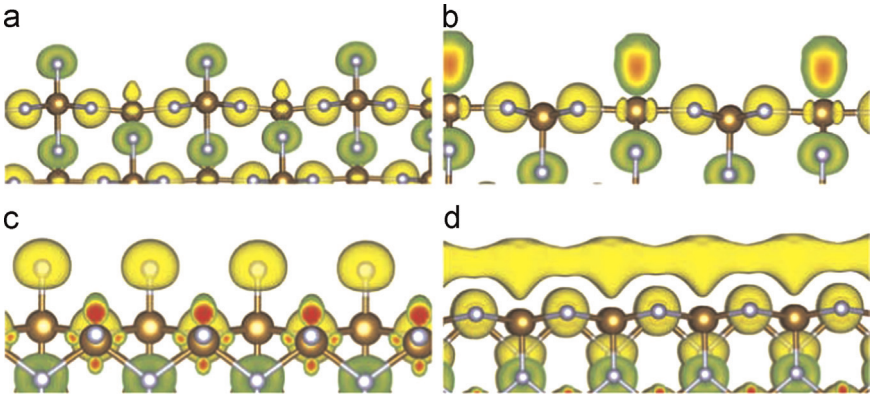

Fig. 7. Electron localization function for the lowest energy surfaces. (a) and (c) correspond to the F-terminated surface along the [100] and [010] planes, respectively. (b) and (d) correspond to the Fe-terminated surface along the [100] and [010] planes. Light colors correspond to F while darker ones correspond to Fe. (For interpretation of the references to color in this figure caption, the reader is referred to the web version of this paper.)

since one Fe atom cannot form a F–Fe–F trimer. Therefore it has a stronger bonding with its second neighbors, while the bonding of the lateral F–Fe–F trimer is weaker, which is responsible for the appearance of the large electron localization function along the [010] direction.

4. Conclusions

Due to the importance of (110) surface of iron fluoride for the exchange bias phenomenon, we investigated it using *ab initio* techniques. We calculated the surface energy, magnetic moment, band structure, charge density and electron localization function. The two possible terminations (Fe and F) were investigated. A detailed comparison with the bulk has been performed and significant differences have emerged. The FeF_2 surface reconstruction determines the atomic and electronic structure of the free surface. For example, for the Fe terminated surface metallic surface states emerge, yielding changes in the electric conductivity. Moreover, this surface develops magnetism of a magnitude of $0.1\mu_B$ per surface unit cell. The charge density shows important changes, which are limited to the first layer, but which also modify the bonding in the vicinity of the surface. While its role in EB is debatable the net magnetic moment that develops on the surface is expected to play a significant role in the understanding of the EB phenomenon.

Acknowledgments

Supported by the Fondo Nacional de Investigaciones Científicas y Tecnológicas (FONDECYT, Chile) under grants 11110510 and 1150806 (F.M.), 1130672 (J.M.L.), 3140526 (R.G.), 1120399 and 1130272 (M.K.), Financiamiento Basal para Centros Científicos y Tecnológicos de Excelencia, Chile, the Donors of the American Chemical Society Petroleum Research Fund for partial support of this research under Contract 54075-ND10 (A.R.), Texas A&M University – CONACyT collaborative research program (I.V.R. and A.H. R.), and Texas A&M University (I.V.R.). We acknowledge the use of Extreme Science and Engineering Discovery Environment (XSEDE) supported by National Science Foundation Grant no. OCI-1053575. Furthermore, for providing HPC resources, the authors acknowledge Texas Advanced Computing Center (TACC) at the University of Texas at Austin, and Super Computing System (Mountaineer) at WVU, funded in part by the National Science Foundation EPSCoR Research Infrastructure Improvement Cooperative Agreement 1003907, the state of West Virginia (WVEPSCoR via the Higher Education Policy Commission), and WVU.

References

[1] B. Dieny, V.S. Speriosu, S. Metin, S.S.P. Parkin, B.A. Gurney, P. Baumgart, D. R. Wilhoit, J. Appl. Phys. 69 (1991) 4774.
[2] B. Dieny, V.S. Speriosu, S.S.P. Parkin, B.A. Gurney, D.R. Wilhoit, D. Mauri, Phys. Rev. B 43 (1991) 1297.
[3] J. Nogués, I.K. Schuller, J. Magn. Magn. Mater. 192 (1999) 203 (and references therein).
[4] W.P. Meiklejohn, C.P. Bean, Phys. Rev. 102 (1956) 1413.
[5] W.P. Meiklejohn, C.P. Bean, Phys. Rev. 105 (1957) 904.
[6] M. Kiwi, J. Magn. Magn. Mater. 234 (2001) 584 (and references therein).
[7] H. Ohldag, H. Shi, E. Arenholz, J. Stöhr, D. Lederman, Phys. Rev. Lett. 96 (2006) 027203 , URL ⟨http://link.aps.org/doi/10.1103/PhysRevLett.96.027203⟩.
[8] J. Nogués, C. Leighton, I.K. Schuller, Phys. Rev. B 61 (2000) 1315.
[9] E. Arenholz, K. Liu, Z. Li, I.K. Schuller, Appl. Phys. Lett. 88 (2006) 072503.
[10] R. Morales, Z.-P. Li, J. Olamit, K. Liu, J.M. Alameda, I.K. Schuller, Phys. Rev. Lett. 102 (2009) 097201 , URL ⟨http://link.aps.org/doi/10.1103/PhysRevLett.102.097201⟩.
[11] B. Kagerer, C. Binek, W. Kleemann, J. Magn. Magn. Mater. 217 (2000) 139 (ISSN 0304-8853), URL ⟨http://www.sciencedirect.com/science/article/pii/S0304885300003152⟩.
[12] S. Roy, M.R. Fitzsimmons, S. Park, M. Dorn, O. Petracic, I.V. Roshchin, Z.P. Li, X. Batlle, R. Morales, A. Misra, et al., Phys. Rev. Lett. 95 (2005) 047201.
[13] M.R. Fitzsimmons, B.J. Kirby, S. Roy, Z.P. Li, I.V. Roshchin, S.K. Sinha, I. K. Schuller, Phys. Rev. B 75 (2007) 214412.
[14] K. Badgley, M. Erekhinsky, I.K. Schuller, M. Zhernenkov, M.R. Fitzsimmons, C. W. Miller, I.V. Roshchin, Bull. Am. Phys. Soc. 55 (2) (2010) D34.00009 (APS March Meeting).
[15] I.V. Roshchin, K. Badgley, K. Belashchenko, M. Zhernenkov, M.R. Fitzsimmons, I.K. Schuller, Bull. Am. Phys. Soc. 55/56 (2) (2011) V16.2 (APS March Meeting).
[16] I.V. Roshchin, K.E. Badgley, M. Zhernenkov, M.R. Fitzsimmons, M. Varela, S.J. Pennycook, Z.-P. Li, H. Ponce, A.H. Romero, C.W. Miller, et al., in: 2010 Proceedings of the 12th International Conference on Electromagnetics in Advanced Applications, ICEAA'10, September 20–24, 2010, IEEE Computer Society, 2010, p. 631.
[17] H. Yamazaki, J. Satooka, J. Phys.: Condens. Matter. 15 (2003) 1201.
[18] J. Mattsson, C. Djurberg, P. Nordblad, J. Magn. Magn. Mater. 136 (1994) L23 (ISSN 0304-8853), URL ⟨http://www.sciencedirect.com/science/article/pii/0304885394904405⟩.
[19] S. López-Moreno, A.H. Romero, J. Mejía-López, A. Muñoz, I.V. Roshchin, Phys. Rev. B 85 (2012) 134110 , URL ⟨http://link.aps.org/doi/10.1103/PhysRevB.85.134110⟩.
[20] J. Nogués, D. Lederman, T.J. Moran, I.K. Schuller, K.V. Rao, Appl. Phys. Lett. 68 (1996) 3186.
[21] D. Lederman, J. Nogués, I.K. Schuller, Phys. Rev. B 56 (1997) 2332.
[22] J. Nogués, T.J. Moran, D. Lederman, I.K. Schuller, Phys. Rev. B 59 (1999) 6984.
[23] M. Kiwi, J. Mejía-López, R.D. Portugal, R. Ramírez, Appl. Phys. Lett. 75 (1999) 3995.
[24] M. Kiwi, J. Mejía-López, R.D. Portugal, R. Ramírez, Solid State Commun. 116 (2000) 315.
[25] R. Morales, M. Vélez, O. Petracic, I.V. Roshchin, X. Batlle, J.M. Alameda, I. K. Schuller, Appl. Phys. Lett. 95 (2009) 092503.
[26] G. Kresse, J. Furthmüller, J. Comput. Mater. Sci. 6 (1996) 15.
[27] G. Kresse, J. Furthmüller, Phys. Rev. B 54 (1996) 11169.
[28] J.P. Perdew, K. Burke, M. Ernzerhof, Phys. Rev. Lett. 77 (1996) 3865.
[29] P. Blöchl, Phys. Rev. B 50 (1994) 17953.
[30] G. Kresse, D. Joubert, Phys. Rev. B 59 (1999) 1758.
[31] V.I. Anisimov, F. Aryasetiawan, A.I. Lichtenstein, J. Phys.: Condens. Matter 9 (1997) 767.
[32] S.L. Dudarev, G.A. Botton, S.Y. Savrasov, C.J. Humphreys, A.P. Sutton, Phys. Rev. B 57 (1998) 1505.

[33] J. Spray, U. Nowak, J. Phys. D: Appl. Phys. 39 (2006) 4536.
[34] T. Mewes, B. Roos, S. Demokritov, B. Hillebrands, J. Appl. Phys. 87 (2000) 5064.
[35] N. Nakagiri, M.H. Manghnani, Y.H. Kim, C.L. Ming, High-Pressure Research in Mineral Physics, 1st ed., Terra Scientific, Tokyo, Japan, 1987.
[36] P.E. Blöchl, O. Jepsen, O.K. Andersen, Phys. Rev. B 49 (1994) 16223 , URL ⟨http://link.aps.org/doi/10.1103/PhysRevB.49.16223⟩.
[37] J. Strempfer, U. Rütt, S.P. Bayrakci, T. Brückel, W. Jauch, Phys. Rev. B 69 (2004) 014417.
[38] J. Kushauer, C. Binek, W. Kleemann, J. Appl. Phys. 75 (1994) 5856.
[39] C. Binek, Ising-type antiferromagnets: model systems in statistical physics and the magnetism of exchange bias, in: Springer Tracts in Modern Physics, Springer, Berlin, 2003.
[40] M. Lederman, J.M. Hammann, R. Orbach, Physica B 165–166 (1990) 179.
[41] A.S. Borovik-Romanov, Sov. Phys. JETP 11 (1960) 786.
[42] S. Mu, K. Belashchenko, Bull. Am. Phys. Soc. 58/59 (1) (2014) H1.296 (APS March Meeting).